Thickness metrology and end point control in W chemical vapor deposition process from SiH$_4$/WF$_6$ using *in situ* mass spectrometry

Y. Xu,[a)] T. Gougousi,[b)] L. Henn-Lecordier, Y. Liu, S. Cho, and G. W. Rubloff[c)]
Department of Materials and Nuclear Engineering, and the Institute for Systems Research,
University of Maryland, College Park, Maryland 20742

Real-time, *in situ* chemical sensing has been applied to achieve reaction metrology and advanced process control in a low pressure tungsten chemical vapor deposition process based on WF$_6$ and SiH$_4$ reactants (silane reduction process). Using mass spectrometry as the sensor to detect both product generation (H$_2$) and reactant depletion (SiH$_4$) at wafer temperature of 200–250 °C, these signals provided a direct real-time measurement of deposited film thickness with an uncertainty less than 2%, and this thickness metrology signal was employed to achieve real-time process end point control. When reactant conversion rates are sufficient (~20% in this case) as often occurs in manufacturing processes, the thickness metrology (1.0%–1.5%) and control (~1.5%–2.0%) accuracies are in the regime needed for meaningful application of advanced process control. Since the *in situ* sensor delivers a metrology signal in real time, real-time process control is achieved, enabling compensation for random process disturbances during an individual process cycle as well as for systematic wafer-to-wafer process drifts. These results are promising for manufacturing from the standpoints of metrology accuracy and application in real-time control. © *2002 American Vacuum Society.* [DOI: 10.1116/1.1520555]

I. INTRODUCTION

A. Advanced process control (APC)

Process control based on advanced metrology has been considered a key to manufacturing and equipment productivity in the semiconductor industry for some time.[1] With increasing attention on the issues of capital productivity and the advent of the 300 nm wafer generation, advanced process control (APC) has attracted even more attention.[2–7] Sensor-driven and model-based, APC can be thought of as the confluence of two components; (1) course correction, in which process variations are compensated by run-to-run (R2R) or real-time control in order to maintain produce quality; and (2) fault management, in which equipment and process faults are detected, classified, predicted, and corrected through equipment repair. Significant advances in implementing APC in manufacturing have been made in both domains.

Fault detection using real-time, *in situ* [e.g., mass spectrometry or residual gas analysis (RGA)] has been particularly effective in detecting known fault mechanism and initiating corrective actions, typically associated with equipment repair;[8,9] for example, failure to adequately purge gas manifolds when replacing gas sources can lead to serious gas line contamination, which is easily detected using an RGA and remedied through proper purging. Because equipment downtime involves huge costs to the fab, knowing the common fault mechanisms which can be caught in such ways and deploying real-time detection of such faults has a

major payback. Typically, the sensor signals to trigger such fault detection does not demand high quantitative accuracy, because repair actions may be triggered simply on the clear existence of fault signals.

Course correction has also made progress in manufacturing implementation, primarily on the basis of in-line metrology carried out between process steps, rather than using real-time, *in situ* sensors. In this way, systematic drifts of process equipment can be identified and compensated for through run-to-run (wafer-to-wafer) control approaches. Given the importance of maintaining process centering at each step, and the fact that many process tools [e.g., etch, chemical vapor deposition (CVD)] exhibit systematic drifts associated with intrinsic physics and the chemistry of the reactor, such run-to-run control offers major payback in manufacturing as well.

B. Real-time, *in situ* sensors

Real-time, *in situ* sensors have the potential to deliver substantial further value from APC if implemented in manufacturing. In terms of course correction, they could drive real-time as well as run-to-run control, thereby allowing course correction within the current process/wafer and enabling compensation not only for systematic longer-term process drift, but also for random variations in process on a time scale within that of a single-wafer process itself. In addition, the same sensors may also implement and potentially improve fault management, carrying out the fault detection described above and also enabling a higher sensitivity to fault mechanisms for more pervasive fault management benefits.

Several *in situ* gas sensing methods have been investigated in chemical processes for silicon technology, including

Fourier transform infrared spectroscopy,[10,11] UV spectroscopy,[12] acoustic sensing,[13,14] and quadrupole mass spectrometry (QMS). QMS has long been recognized as an excellent sensor for leak detection and contamination control, and it has become a workhorse for fault detection as described above. Owing to its high chemical sensitivity and selectivity, QMS is capable of providing extensive time-dependent information regarding process state and wafer state metrics. Its application has been expanded to a wide variety of semiconductor device manufacturing processes ranging from end point detection in dielectric etching[15] to film thickness metrology during CVD processes for gate oxide[16] and metallization.[17]

Our research has been aimed at developing real-time, *in situ* sensor methodologies which employ chemical sensors as quantitative monitors of both process state and wafer state, with QMS the primary sensor employed in this work. While normally considered a process state sensor, we have demonstrated in silane-based rapid thermal CVD and plasma enhanced CVD (PECVD) processes and in W CVD that quantitative measurements of product generation and reactant depletion provide a thickness or deposition rate metrology based on mass balances, thus producing a wafer state sensor in concert with process sensing. The primary goal has been to improve the accuracy of this real-time, *in situ* sensor-based metrology to a sufficient level, probably 1%–2%, that it may deliver value in high volume manufacturing, either in run-to-run control and/or in real-time control.

C. W CVD process sensing, metrology, and control

Our recent work on W CVD process sensing, metrology, and control[17] showed that the time integration of HF generation and H_2 depletion signals from mass spectrometry in a low-pressure (sub-torr), selective W CVD process using H_2 reduction:

$$3H_2 + WF_6 \Leftrightarrow 6HF(g) + W(s), \tag{1}$$
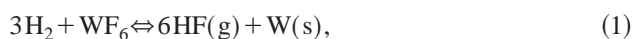
provides a measurement of the W film thickness. In this case the HF generation signal showed an error of about 7% limited mainly by the poor utilization of the reactants (around 3%) in the low process pressure regime. Since CVD manufacturing processes usually involve considerably higher reactant utilization, it is expected that better thickness metrology should be achievable in manufacturing.

To obtain higher conversion rates in W film deposition, two approaches were considered, (1) processing wafer at higher pressure and temperature, and (2) replacing H_2 with SiH_4, a more efficient reducing agent. Because our Ulvac 1000 process tool was currently limited to the sub-torr pressure regime by the configuration of the equipment, the second approach was adopted. The overall reaction equation of the SiH_4 reduction process[18] is

$$3SiH_4 + 2WF_6 \Leftrightarrow 6H_2(g) + 2W(s) + 3SiF_4(g). \tag{2}$$

Thus in this work we sought to monitor different product species (H_2, SiF_4) compared to the previous study of H_2 reduction. Because the deposition of every two W atoms consumes three SiH_4 molecules and produces six H_2 and three SiF_4 molecules, the variations of the reactant and product partial pressures should be directly correlated to the deposited W film thickness.

The results demonstrate that at higher reactant utilization levels as expected in manufacturing, mass spectrometry sensing provides a real-time thickness metrology with an accuracy of about 2%, i.e., in the range needed for manufacturing, and that it can be used to achieve real-time end point control of the film thickness at a comparable level. This opens the door to real-time APC applications in manufacturing, with the capability to compensate within-wafer random process variations as well as longer-term systematic wafer-to-wafer process drifts.

II. EXPERIMENT

The processes were carried out on an Ulvac-ERA 1000 W-CVD cluster tool, a single-wafer, cold wall system with lamp heating for the wafer. The tool was designed for selective W-CVD process from SiH_4/WF_6 mixture below 1 Torr. The process parameters were pressure: 0.1 Torr; nominal temperature: 200–250 °C; SiH_4 flow rate: 8 sccm; WF_6 flow rate: 10 sccm, and Ar flow rate: 180 sccm. It was found that polycrystalline α-W formed at $P(SiH_4)/P(WF_6) < 1$. Increasing the ratio to higher values resulted in W film consisting of a mixture of α-W and β-W,[19] which is of high electrical resistivity. Therefore in this research a SiH_4/WF_6 flow rate ratio was kept fixed at 0.8.

To obtain the film thickness metrology from the time integration of mass spectrometry signals, 37 wafers were processed for different deposition times, varying between 40 and 180 s.

Once a correlation between film thickness and integrated mass-spectrometry signals were established, two more sets of experiments were carried out to test real-time end point control. In the first set of experiments, the recipe process parameters were kept fixed, while in the second set, a systematic temperature drift was introduced as a process disturbance. For both cases, the H_2 generation signal was monitored and integrated over time as an indicator of W film thickness, based on the metrology results obtained before. The process was terminated as soon as the time integrated H_2 signal reached the target value. Then the actual W film thickness was measured offline to validate metrology.

A direct gas sampling system was implemented just downstream of the wafer, in the process chamber for real-time *in situ* chemical sensing using an Inficon™ H200M CIS mass spectrometer. To minimize wall reactions in which WF_6 and HF condense on the stainless steel surface at room temperature, the wall area of the sampling system was kept minimal and the sampling manifold was heated at 60 °C. The drag stage of the turbopump in the gas sampling system was used to withdraw gas dynamically from the process chamber through the sampling system in order to improve the response time of the sampling, enabling a short response time ($\sim$3 s). Refer to Ref. 17 for more information regarding this sampling system. During the process, the pressure in the

manifold of the sampling system was about 4×10^{-7} Torr. Electron multiplier detection was used at an acceleration voltage of 1000 V to enhance the signal-to-noise ratio. Throughout the whole period of the experiment, the mass spectrometer exhibited extremely stable sensitivity. As monitored through the Ar^+ signal (40 amu), the mass spectrometer sensitivity varied by less than 1% to 2% over 2 months, which contributed greatly to the success in metrology development.

Initially, bare 4 in. Si wafers were used for W deposition from a mixture of SiH_4/WF_6. However, under these conditions the W film was prone to flaking due to its poor adhesion to the bare silicon (Si) wafer. An expedient solution was to use Si wafers previously covered with a layer of W film 1000–2000 Å thick (obtained from earlier H_2 reduction processes). This way, W films as thick as 3000 Å were successfully obtained by SiH_4 reduction. Since the underlying W film had gone through different H_2 reduction processes, the surface conditions of these W-capped wafers varied one from each other, inducing significant random variations of the growth rates from run to run. However, this also provided a perfect scenario to demonstrate the benefit of sensor-based real-time control.

A STYLUS™ microbalance was employed to measure the film weight after the deposition process at a resolution of 10^{-4} g, which corresponds to a thin W layer of 6.6 Å on a 4 in. wafer, or less than 0.5% of the film weight deposited in most runs. From the film weight, the average thickness can be estimated from the known wafer area (4 in. wafer) and W density (19.3 g/cm^3). This proved to be a faster and more accurate way of determining the average film thickness compared to lithograph patterning and profilometry. At this stage, we were not overly concerned with across-wafer thickness uniformity.

III. RESULTS

SiH_4 is such an efficient reducing agent that reaction rates for the SiH_4 reduction process are significantly enhanced compared to those for H_2 reduction at relatively low temperature and pressure conditions of 250 °C and 0.1 Torr. The measured deposition rate was about 1100 Å/min,[20] i.e., a $5\times$ improvement over the H_2 reduction processes at 500 °C and 0.5 Torr. The corresponding WF_6 depletion rate was estimated at around 20% based on the measured W film weight.

Figure 1 depicts the mass spectrometry signals for species at 2 amu (H_2^+), 30 amu (SiH_2^+), and 85 amu (SiF_3^+) recorded in a typical SiH_4 reduction process, where SiH_2^+ and SiF_3^+ are fragments produced by ionization of SiH_4 and SiF_4, respectively. Each process consisted of two steps: a cold wafer cycle for background measurement and a hot wafer cycle for film deposition. In the cold wafer cycle, the same amount of reactants was inlet into the reactor as in the hot deposition cycle, but the wafer was not heated. The high temperature reaction of the precursor with SiH_4 that produces H_2 and SiF_4 resulted in a significant increase of H_2^+ and SiF_3^+ (reac-

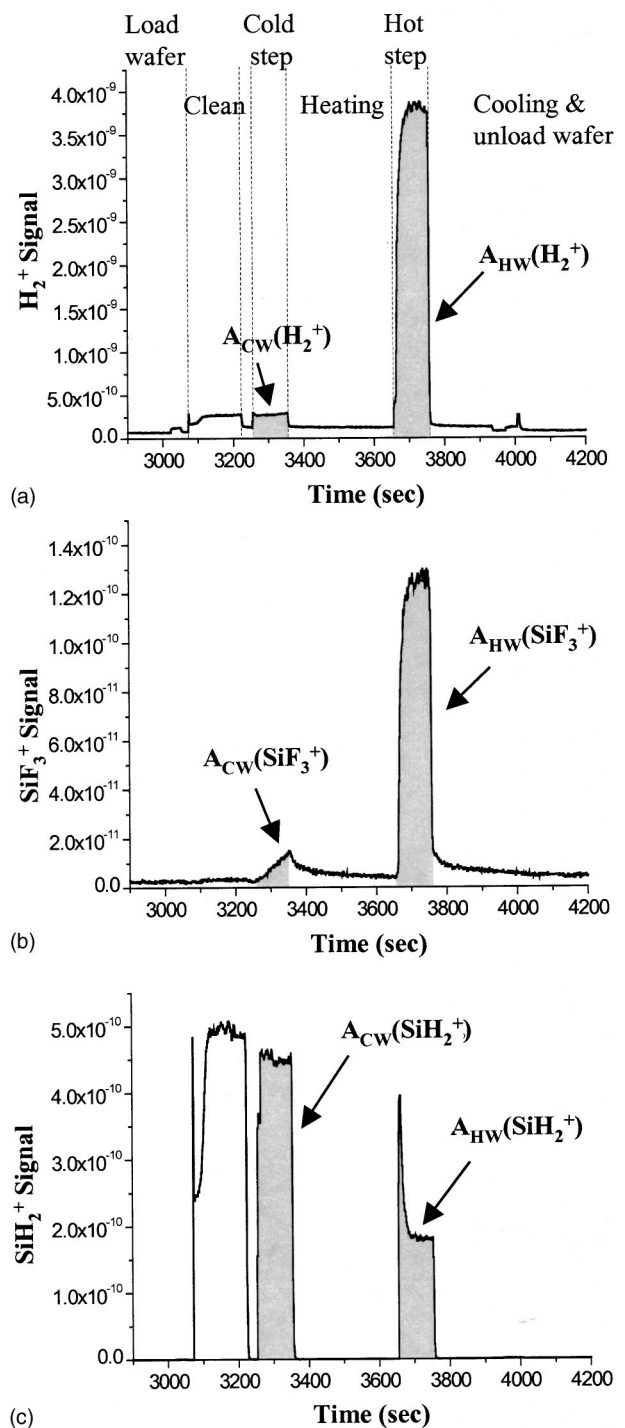
FIG. 1. Time evolution of H_2^+, SiF_3^+, and SiH_2^+ mass spectrometry signals in a typical SiH_4 reduction W-CVD process. (a) and (b) are, respectively, related to H_2 and SiF_4 generated products (c) to SiH_4 depleted reactant.

tion product signals corresponding to H_2 and SiF_4, respectively), while the decrease of the SiH_2^+ signal logically showed the depletion of the reactant SiH_4.

The response of the downstream mass spectrometry sensor system is of order 1–3 s,[17] so that the time dependence seen in Fig. 1 reflects dynamics intrinsic to the equipment design and the process carried out in it. Longer time con-

stants, e.g., those indicated in the early stage of the hot step, reflect primarily equipment dynamics such as the reactor residence time that determines how long it takes after initiating reactant admission to produce steady-state values in the reactor for reaction product concentration and depleted reactant levels. In principle these dynamic effects will influence the linearity with which our sensor signals reflect actual deposition rates and thicknesses. Indeed, we have seen notable effects on the metrology, particularly when the process recipe does not enable attainment of steady state; in such cases, dynamic simulation of equipment and process provides a mean to understand and perhaps correct for these effects. In most cases, however, the metrology data which relates real-time chemical sensing signals to postprocess thickness measurements, as presented below, demonstrates that these effects are modest. Furthermore even if nonlinearities are present in the metrology, manufacturing processes strive to operate at a fixed process design point and recipe for many wafers, so the metrology needed is confined to a narrow range of variation which will then be quite linear.

In contrast to the H_2 reduction process for W CVD in the sub-torr regime,[17] the H_2^+ and SiF_3^+ reaction product signals are quite small in the cold wafer cycle, only about 10% of the corresponding signals in the hot wafer cycle. Since the reaction product signals during the cold cycle are indicators of the reactor and mass-spectrometer chemical background, this suggests a high conversion rate from reactions on the wafers compared to room-temperature wall reactions. During the cold wafer cycle, the H_2^+ signal is quite stable, while the SiF_3^+ signal exhibits an upward drift. This H_2^+ background, seen when the wafer is cold, results mainly from the ionization-related fragmentation of the reactant SiH_4. In contrast, the SiF_3^+ background comes from SiF_4, which is formed in moderate amounts during the cold cycle by wall reaction and/or ion–molecule reactions in the ionizer of the mass spectrometer. As a reaction product generated at cold surfaces of the reactor system, it takes time for the SiF_4 signal to reach equilibrium.

The metric defined for the W film thickness using a H_2 generation signal can be expressed by

$$S_{H_2} = A_{HW}(H_2) - A_{CW}(H_2), \tag{3}$$

where A is the area beneath the H_2^+ signal, i.e., the time-integrated H_2^+ signals, and HW and CW refer to the hot and cold wafer cycles, respectively.

Similarly, the metrics based on the SiF_3^+ signal can be formulated by

$$S_{SiF_3} = A_{HW}(SiF_3) - A_{CW}(SiF_3). \tag{4}$$

For the SiH_2^+ reactant depletion signal, a slightly different expression was used:

$$S_{SiH_2} = \frac{A_{HW}(SiH_2) - A_{CW}(SiH_2)}{A_{CW}(SiH_2)} \times t. \tag{5}$$

Since SiH_4 is a reactant which is depleted by the deposition reaction, this quantity is normally negative (though for convenience its absolute value is plotted below). As a reactant, a considerable SiH_2^+ background was present in the cold wafer cycle, therefore the signal was normalized to the SiH_2^+ "cold wafer" area [the division by A_{CW} in Eq. (5)] to compensate for any change in the incoming reactant flux, and this quantity was multiplied by the deposition time t to compensate for any change in the time period of the process from one run to the next. These calculations deliver a sensor-based thickness metrology over the time t.

A total of 37 wafers were processed in the same way, but with varying deposition times, for which results are shown in Fig. 2. Linear relationships with correlation coefficient (R^2) larger than 99% were established between the film thickness and the integrated mass spectrometry signals for S_{H_2}, S_{SiF_3}, and S_{SiH_2} [derived from Eqs. (3), (4), and (5)], and among these S_{H_2} gave the best fit to the actual film weight (see Fig. 2). Since the SiH_4 reduction process was carried out on wafers already carrying a W film, no anomalies were observed related to the initial deposition and nucleation, and all three curves in Fig. 2 extrapolate through the origin. In contrast, H_2 reduction experiments with deposition directly on the Si surface showed anomalies associated with a dominant initial nucleation step (Si reduction), which formed the initial W layer but generated a different reaction product than that monitored for the H_2 reduction process.[17] Furthermore, almost no first wafer effect was observed, with the single exception shown in Fig. 2(c).

Figure 3 shows the relative error in ion mass spectrometry based metrology, determined as error of S_{H_2} from the regression fit in the metrology calibration for the 37 wafers shown in Fig. 2(a). The average error and standard deviation in the film thickness measurement as obtained from real-time, *in situ* mass spectrometry are 1.25% and 1.09%, respectively.

Due to the high reactant utilization rates of this SiH_4 reduction process and the resulting high ratio of generated product to background signals, analysis was also carried out ignoring corrections associated with the background as measured from the unheated (cold) wafer cycle. The hot wafer signal $A_{HW}(H_2)$ alone is plotted versus actual film thickness determined postprocess in Fig. 4. In this figure, runs for 37 wafers (solid data points) actually included a cold wafer cycle in the process (though it was not used for calculating the metrology signal), while runs for ten wafers (open data points) did not include any cold wafer cycle in the process cycle. This approach to investigating a thickness metrology signal dependent only on the hot wafer portion is motivated by the recognition that manufacturing application would preclude a step in the process cycle to measure a cold wafer background.

Figures 2 and 4 demonstrate a strong correlation between integrated mass spectrometry signals and actual postprocess film weight (thickness) measurements for the SiH_4 reduction process for W CVD. To better assess the thickness metrology results, the residual for each data point was calculated, defined as the difference between the actual y values for each data point and the values resulting from the linear regression fitting. Then the absolute value of the residual was divided
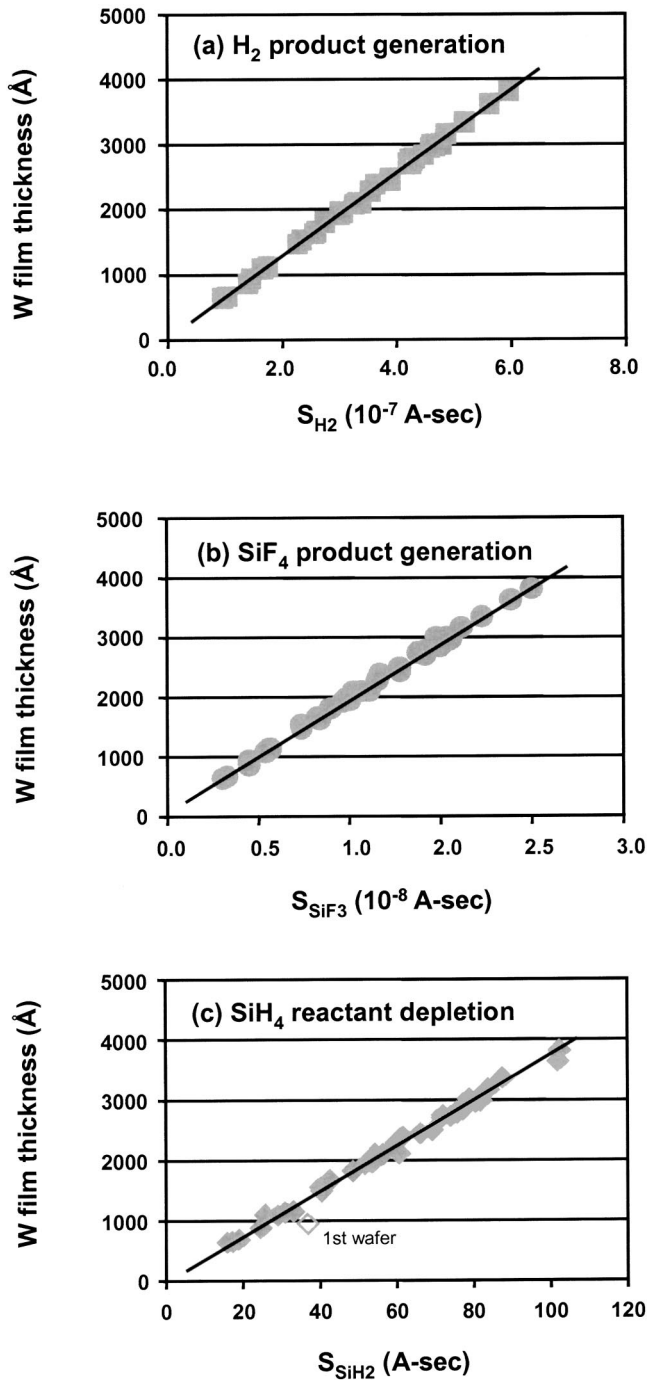
FIG. 2. Film thickness metrology results from S_{H_2}, S_{SiF_3}, and S_{SiH_2} for 37 wafers processed at 250 °C and different deposition times. S_{H_2}, S_{SiF_3}, and S_{SiH_2} are, respectively, derived from Eqs. (3), (4), and (5), such that the background during the cold wafer sequence (prior to deposition) is taken into account. Note that for (c) the absolute value of the quantity S_{SiH_2} defined in Eq. (5) is used.
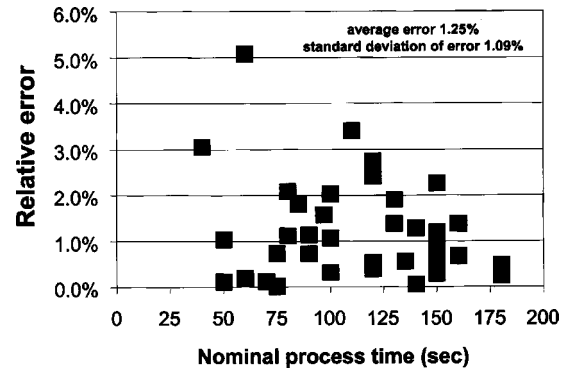

FIG. 3. Relative error in mass spectrometry based metrology, determined as error of S_{H_2} from the regression fit in the metrology calibration for the 37 wafers shown in Fig. 2(a). The average error and standard deviation in the film thickness measurement as obtained from real-time, *in situ* mass spectrometry are 1.25% and 1.09%, respectively.

is used. The H_2 product generation signal provides the most accurate real-time thickness metrology for the SiH_4 reduction process for W CVD as investigated here.

Furthermore, the H_2 product generation signal provides nearly as accurate a thickness metrology using only the hot wafer signal [from $A_{HW}(H_2)$] as does the more complex (and manufacturing incompatible) approach which includes a cold wafer cycle. Therefore in the succeeding W film thickness real-time end point control experiments all wafers were processed without a cold wafer cycle. Unless otherwise noted, H_2 generation signals in the following sections all refer to the quantity $A_{HW}(H_2)$, instead of S_{H_2}. For process control investigations, $A_{HW}(H_2)$ was taken as the control variable, i.e., the sensor-derived signal employed to drive the control methodology.
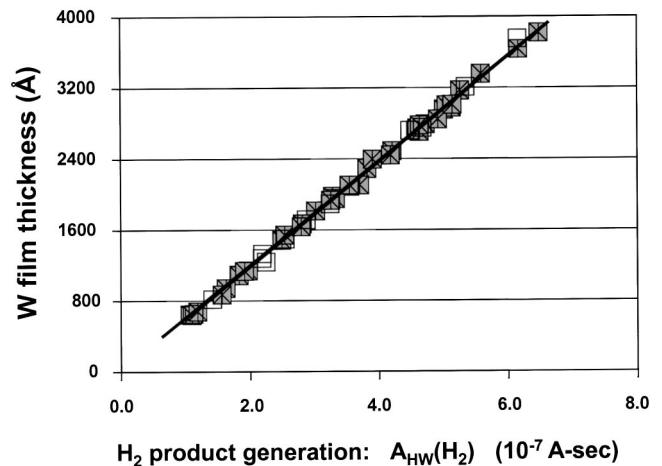

FIG. 4. Metrology results from $A_{HW}(H_2)$ in the SiH_4 reduction W-CVD process. $A_{HW}(H_2)$ is calculated from the integrated H_2 signal during the deposition step *without* taking into account the background during the cold wafer sequence. The solid data points represent $A_{HW}(H_2)$ calculated from the 37 initial runs. The open data points were obtained from ten additional runs whose process recipes did not include a cold wafer cycle.

by the measured true value to obtain the relative error. Table I summarizes the average and standard deviation of the metrology results for the 37 wafers. For thickness metrology derived from either the H_2 or the SiF_4 product generation signals, the error is less than 2%, while the error is somewhat higher (2.5%–3.0%) when the SiH_4 reactant depletion signal

TABLE I. Statistical analysis of the integrated mass-spectrometry signals in the SiH_4 reduction process for 37 wafers. S_{H_2}, S_{SiF_3}, and S_{SiH_2} are, respectively, derived from Eqs. (3), (4), and (5) where the integrated area during the cold wafer sequence (prior to deposition) is taken into account. $A_{HW}(H_2)$ refers to the integrated H_2 signal during the deposition step in which the wafer was heated, without taking into account any background measurement involving a cold wafer.

Metrology error	Using reaction products			Using reactant depletion
Chemical species	H_2		SiF_4	SiH_4
Metric	S_{H_2}	$A_{HW}(H_2)$	S_{SiF_3}	S_{SiH_2}
Average error	1.25%	1.55%	1.86%	2.83%
Standard deviation of error	1.09%	1.38%	1.38%	2.59%

IV. REAL-TIME END POINT PROCESS CONTROL

Sensor-based film thickness metrology is a prerequisite for advanced process control of deposition thickness. The primary goal of this research is the development of real-time, *in situ* chemical sensors as required to achieve real-time advanced process control. Results in the previous section show that W film thickness metrology can be obtained in the SiH_4 reduction W-CVD process from time integration of mass spectrometric sampling signals associated with H_2 and/or SiF_4 product generation, as well as from SiH_4 depletion signals. Indeed, these thickness metrology signals deduced from H_2 or SiF_4 product generation are promising in two respects: (1) their accuracy, of the order of 1.5%–2.0%, is viable to add value in manufacturing; and (2) because they are obtained in real time, they could be used to drive either run-to-run (wafer-to-wafer) or real-time process control.

Mass spectrometry based thickness metrology was employed for run-to-run control in our previous research, a H_2 reduction process for W CVD at low pressure (<1 Torr).[21] In this case, low reactant conversion rates limited the metrology to 7%, and in turn this provided a significant constraint on the value which could be obtained from run-to-run control.

With the significantly higher reactant utilization levels achieved by the SiH_4 reduction process in this work, a much improved metrology accuracy (1.5%–2.0%) is achieved. Here we use this real-time, *in situ* thickness metrology to drive real-time end-point process control: the sensor signals are captured and processed in real time, and when the desired value of the integrated sensor signal is achieved, the process is terminated. Thus the objective is to stop the process when the target thickness is reached (end point control), rather than to modify process parameters during the process. Assuming suitable sensor/metrology technology is available, real-time process control offers two major advantages over run-to-run control: (1) it may be simpler to implement, avoiding complex algorithms which deduce trends from run-to-run measurements; and (2) it may compensate not only for long-term systematic process drifts (as is the goal of run-to-run control), but also for random variations within the process cycle for each wafer.

Experiments were carried out with batches of 8–10 wa-

fers each, using H_2 product signals as the control variable and terminating the process time such that the integrated H_2 product signal matches its target value. The initial wafer was processed over a deposition time of 150 s. The H_2 generation signal was integrated over that period as described previously to determine the target value $A_{HW}(H_2)_{[0]}$. Subsequent wafers in the batch were processed until the corresponding integrated product signals $A_{HW}(H_2)$ reached the target $A_{HW}(H_2)_{[0]}$, at which point the process was stopped. Thus the deposition time served as the primary controlled variable, and the film thickness became the secondary controlled variable (measured postprocess from wafer weight measurements). Given that the real-time sensor signal is not a direct measurement of the desired property (which is the actual film thickness), the degree to which both the integrated sensor signal [$A_{HW}(H_2)$ over the process cycle] and the actual film thickness were controlled are important results for assessing this approach.

As a further evaluation, experiments were done in two ways, (1) with each wafer subjected to the same process recipe, and (2) with successive wafers subjected to intentional changes in nominal process temperature to simulate a long-term (run-to-run, or wafer-to-wafer) process drift.

A. Process control experiments at fixed temperatures

Experiments were carried out on batches of wafers without or with the imposition of sensor-based real-time end point control, with results shown in Fig. 5 for the sensor signal $A_{HW}(H_2)$ deduced from H_2 product generation [Fig. 5(a)] and for the actual film thickness determined postprocessing [Fig. 5(b)]. All wafers experienced the same process recipe, i.e., deposition time equal to 150 s at 250 °C.

Results for wafers without end point control are depicted by the open diamonds in Figs. 5(a) and 5(b), labeled ''no control (experiment).'' A random variation of both the mass spectrometry signal and the deposited film thickness of up to 10% is clearly observed. Some of this variation is attributed to different surface conditions of the W-coated starting wafers (described above), but in manufacturing practice such random variations may arise from a number of equipment or process related causes.

In a second batch, real-time end point control was introduced in order to reduce the variations of the film thickness. The target $A_{HW}(H_2)_{[0]}$ for our controlled variable was determined during a first run at 250 °C for 150 s with $A_{HW}(H)_{[0]} = 4.3 \times 10^{-7}$ A s (labeled ''target H_2 value''). The following eight wafers were also processed at 250 °C, but terminated at deposition times which were determined by the condition that the integrated signal $A_{HW}(H_2)$ would match the target $A_{HW}(H_2)_{[0]}$. The closed circles in Figs. 5(a) and 5(b), labeled ''with control,'' represent the sensor signals $A_{HW}(H_2)$ and actual film thicknesses obtained with control. Clearly, real-time end point control substantially improves run-to-run (wafer-to-wafer) thickness control. While this is true in both cases, control of the sensor signal (primary control variable) is somewhat better than that for the actual thickness (secondary control variable), because the latter in-
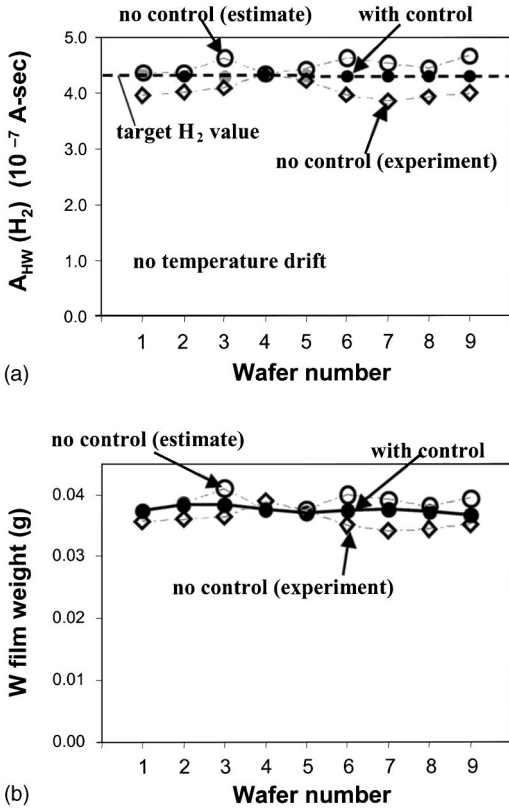
(a)

(b)

FIG. 5. (a) H_2 generation signal $A_{HW}(H_2)$ and W film weight vs run number. The temperature was kept constant at 250 °C. The initial run (150 s) defines the target H_2 value $A_{HW}(H_2)_{[0]}$ of 4.3×10^{-7}. The deposition was terminated for end point control when the mass-spectrometry control signal $A_{HW}(H_2)$ reached $A_{HW}(H_2)_{[0]}$. The closed circles represent $A_{HW}(H_2)$ obtained with process control from a nine-wafer batch; the open circles represent an estimation of $A_{HW}(H_2)$ if the process time had been kept constant (i.e., 150 s) for the same batch. The open diamonds are experimental results from a second batch were no control was introduced (i.e., fixed deposition time for the nine wafers). (b) W film weight vs run number corresponding to the wafers processed with real-time end point control in (a).

volves variations not only from the control methodology but also from the accuracy of the *in situ* metrology.

Since the sensor data during the practice of real-time end point control indicate signal levels during the process, one can estimate what would have been the integrated sensor signals and actual film thicknesses if end point control had not been imposed, i.e., if the same process time (150 s) had been used for all wafers in this second batch. Such a projected $A_{HW}(H_2)$ was calculated as

$$A_{HW}(H_2)_{[projected]} = A_{HW}(H_2)\times[\text{nominal deposition time/}$$
$$\text{actual deposition time}], \quad (6)$$

where the nominal deposition time is equal to the deposition time of the first wafer (i.e., 150 s), and the actual deposition time is that determined for each wafer by the end point control strategy. A projected value of actual film thickness was calculated similarly as
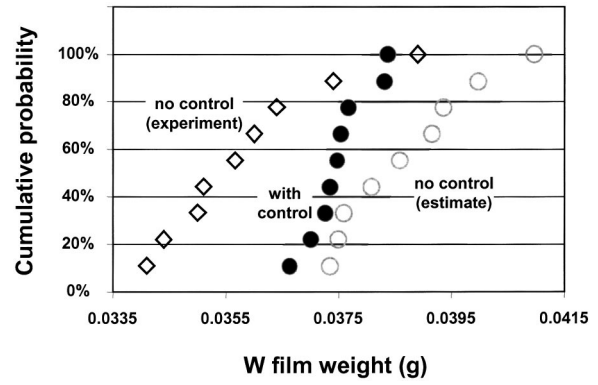

FIG. 6. Cumulative probability of the film weight for two batches of nine wafers processed at constant temperature. The film weights from the process control experiment (closed circles) are distributed over a much narrower weight range than the ones without control (open diamonds). The open circles are an estimate of what the weight distribution would have been if the process time had been kept constant during the process control experiment.

$$\text{W film weight}_{[projected]} = \text{W film weight}$$
$$\times[\text{nominal deposition time/}$$
$$\text{actual deposition time}]. \quad (7)$$

The projected values of the sensor signal and actual film weight are shown as open circles in Figs. 5(a) and 5(b), labeled "no control (estimate)." The variations projected in this way are comparable to those found in the "no control (experiment)" case (open diamonds), again indicating the benefit of real-time end point control. It should be noted that the run-to-run variation in the projected values from the control experiments (open circles) exhibits a different shape, or dependence on wafer number, from that seen for the no-control experiments (open diamonds), since the no-control batch and the control batch both experienced primarily random variations, which would be uncorrelated between two successive wafer batches.

A view of the impact of real-time end point control is shown in Fig. 6 with the cumulative probability distribution of the film weights corresponding to the data in Fig. 5. Note that when end point control is activated (closed circles), the distribution of film weights is much sharper than in the case when no control was imposed (open diamonds) or from the projected values of what would have resulted for the wafers processed with control if the end point control had not been utilized (estimated as described above). It is precisely the sharpening and center stabilization of such distributions which are the goals of advanced process control.

Table II shows a statistical analysis of the deposited film weight results corresponding to the data in Fig. 5. Without end control [corresponding to the data represented by the open circles in Fig. 5, and labeled "no control (estimate)"], the standard deviation of the weight around its average is about 4%. Upon imposing real-time end point control (corresponding to the closed circle data labeled "with control" in Fig. 5, the standard deviation is reduced to 1.6%. Estimates for what these latter values would have been if control were

TABLE II. Statistical analysis of the deposited film weight results for process control experiments carried out at fixed temperature, obtained from two batches of wafers. Batch 1 was processed without control and corresponds to the data represented by the open circles in Fig. 5 [labeled "no control (estimate)"]. Batch 2 was processed using real-time end point control, for which the experimental results correspond to the closed circle data (labeled "with control") in Fig. 6. For batch 2, additional results are given from the estimated weight data which would have occurred if end point control had not been used, corresponding to the open diamonds [labeled "on control (experiment)"] in Fig. 5.
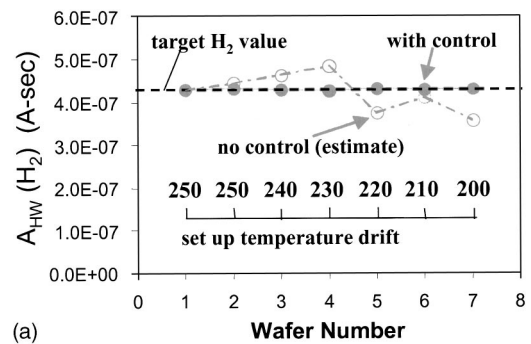
Control error	No control (experiment)	With control	No control (estimate)
Average weight (g)	0.0359	0.0375	0.0387
Standard deviation (g) (%)	0.0015 (4%)	0.0006 (1.6%)	0.0012 (3.1%)

(a)

(b)

FIG. 7. (a) H_2 generation signal $A_{HW}(H_2)$ and W film weight vs run number. A temperature drift of $-10\,°C$ per run was introduced since the third wafer. The solid data points represent $A_{HW}(H_2)$ obtained with real-time control; the open data points indicate the projected $A_{HW}(H_2)$ without control obtained by rescaling the deposition time. (b) W film width vs run number corresponding to the wafers processed with real-time end point control in (a).

not imposed, corresponding to the open circle data in Fig. 5, labeled "no control (estimate)," reveal a standard deviation of 3.1%. For these experiments, with random differences—especially in initial surface conditions—the imposition of real-time end point control achieves significantly improved thickness control and brings the standard deviation into a range which is viable for application in manufacturing.
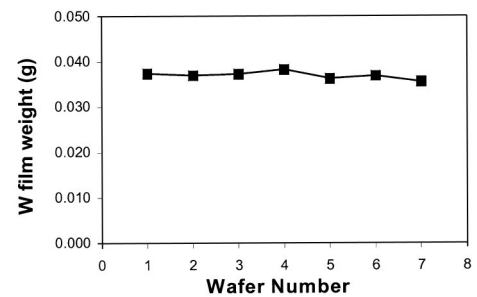
B. Process control experiments using an intentionally introduced temperature drift

In another set of experiments represented in Fig. 7, a systematic temperature drift of $-10\,°C$/wafer was intentionally introduced through modification of the process recipe in order to impose a systematic process drift, using the same mass spectrometry sensor signal target (4.3×10^{-7} A s) as previously used. Nominal temperatures for each wafer are indicated by the scale in Fig. 7(a), with the drift introduced at the third wafer. As described above, real-time end point control was employed [closed data points in Figs. 7(a) and 7(b), labeled "with control"], and in addition a projection of the variations which would have occurred in the absence of the control [open circles in Fig. 7(a), labeled "no control (estimate)"] was made. In addition to the sensor signals in Fig. 7(a), the corresponding consequences on film weight are shown in Fig. 7(b).

Results in Fig. 7 indicate again that the imposition of sensor-based real-time end point control significantly reduces run-to-run (wafer-to-wafer) variability. Despite the addition of an intentional temperature drift of the process from one wafer to the next, random variations dominate: no clear monotonic, systematic drift is observed in the "no control (estimate)" case. Furthermore, one would expect that decreasing temperature with wafer number should reduce the "no control (estimate)" values, since process rates are lower at lower temperatures. It is not clear whether such a drift can be discerned in the Fig. 7(a) data. This may be in part a result of a weak temperature dependence (low thermal activation energy) of the SiH_4 reduction process.

Analysis of the film weight data of Fig. 7(b) is given in Fig. 8 in the form of the relative error (absolute value) relative to the average value. These experiments led to an average error of 2.1%, and a standard deviation of the error of 1.6%. Again, these values are in the range desirable for manufacturing application.

In addition, the data in Fig. 8 do indicate a drift of the data with the intentionally introduced drift nominal wafer temperature, as would be expected for processes which are at least partially thermally activated. It should be noted further that the imposed temperature drift was substantial, i.e., $50\,°C$, which is notably larger than one should expect from
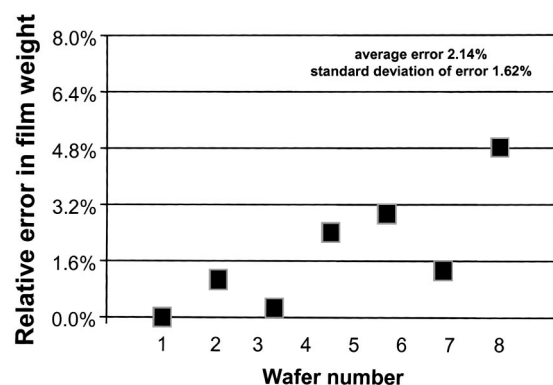

FIG. 8. Relative error (absolute value) of deposited film weight for real-time end point process control experiments corresponding to the data in Fig. 7(b), where an intentional temperature drift was introduced.

process equipment in a manufacturing environment. Such large excursions introduce the possibility of atypical systemic drifts in process behavior, e.g., as wall reactions increase relative to deposition reactions at the wafer surface.

V. DISCUSSION

The primary advance in metrology accuracy obtained using the silane reduction process (rather than hydrogen reduction) for W CVD is attributed to the larger reactant conversion rates using SiH_4. With conversion rates of $\sim 20\%$ for silane reduction, as compared to $\sim 3\%-4\%$ for hydrogen reduction, the product generation and reactant depletion signals associated with deposition are 5 to $6\times$ larger for the silane case, enabling a more accurate deposition rate and/or thickness metrology.

The experiments reported here utilized the H_2 product generation signal to drive real-time end point control. As indicated by the data in Fig. 2 and the summary of metrology errors in Table I, thickness metrology based on the SiF_4 product generation signal is nearly as good as that for H_2. This means that SiF_4 sensing might also be used to drive real-time end point control. The metrology obtained from SiH_4 reactant depletion was not as good (about $2\times$ worse), but nevertheless it is possible that viable metrology signals may be obtained in principle from both reaction product generation and reactant depletion, so that the choice should be made for the specific process application.

A particular advantage of real-time end point control, as opposed to run-to-run control, is that random variations which occur during an individual process cycle—as well as long-term drifts—may be compensated or controlled. While one might have anticipated that the temperature drift per wafer intentionally introduced in the data in Fig. 7(a) would have created a steady decrease of H_2 produce signal with nominal process temperature, it was not observed. Instead, the low thermal activation energy associated with the silane reduction process yielded little, if any, long-term deposition rate drift corresponding to the intentional temperature drift. Instead, variation in process rates, indicated by the H_2 mass spectrometry signal, was rather random from one wafer to the next, and one would further infer that such random process variations occur within an individual process cycle as well. Despite this randomness, the availability of a suitable real-time metrology enabled real-time end point control which permitted excellent control of the mass spectrometry signal, and good control of the resulting film weight in Fig. 7(b), consistent with the accuracy of the metrology itself.

VI. CONCLUSIONS

A real time *in situ* sampling system was implemented in the SiH_4 reduction W-CVD process using mass spectrometry. Real-time mass spectrometry signals from the generation of reaction products (H_2 and SiF_4) and from the depletion of SiH_4 reactant, obtained and integrated through the process cycle, provide a deposition thickness metrology accurate to $1\%-3\%$ when compared to postprocess thickness measurements. In the case of the H_2 product generation signal, the

accuracy of $1\%-1.5\%$ appears viable for real manufacturing applications. These metrology accuracies represent a substantial advance over previous work with the hydrogen reduction process, with the improvement attributed to the significantly higher (5 to $6\times$) reactant conversion rate ($\sim 20\%$) that accompanies silane reduction as cf. hydrogen reduction.

This mass spectrometry based film thickness metrology was further exploited for real-time end point process control. The constructed H_2 generation signal $A_{HW}(H_2)$ was taken as the primary controlled variable. The deposition time was adjusted as the control variable to compensate for random variations as well as systematic long-term process drifts. For a fixed process recipe implemented on a small batch (nine) of wafers, the W layer thickness could be controlled to about 1.5% (standard deviation) based on the real-time thickness metrology signal for the H_2 product, despite the presence of random variations in deposition rates observed in the mass spectrometry signals. This corresponds to the case of control accuracy limited by the metrology accuracy, and the mass spectrometry signals indicated that the imposition of real-time process control in this way significantly improved wafer-to-wafer thickness reproducibility. Additional experiments in which an intentional wafer-to-wafer drift in nominal process temperature was introduced showed similar benefits.

In summary, these results demonstrate that real-time *in situ* chemical sensing by downstream mass spectrometry can deliver real-time thickness metrology and end point control with accuracy of order $1\%-2\%$. We believe this makes the technique viable for manufacturing application, and capable of compensating for random process variations within a process cycle as well as for longer-term (wafer-to-wafer) process variations and systematic drifts. Furthermore, the use of real-time end point control is rather straightforward, particularly in comparison to the various algorithms and models required for implementation of run-to-run control.

It is interesting to speculate on what might be expected from implementation of this methodology in manufacturing. First, the silane reduction process for W CVD has permitted us to experiment with reasonable reactant conversion rates ($\sim 20\%$), and indeed such rates are much closer to those achieved in manufacturing processes (e.g., hydrogen reduction at 10–100 Torr) than the lower values ($3\%-4\%$) we found previously for hydrogen reduction at low pressures (100 mTorr). Second, we expect that a continuously operated process tool in manufacturing would already exhibit more reproducible process behavior than we can obtain in a research environment, thus reducing some of the larger variability sources (e.g., wall reactions) that limit our metrology accuracy. Finally, the specific employment of mass spectrometry to drive metrology and control is synergistic with its already broad use for fault detection in manufacturing: the same sensor system could drive existing fault detection applications and real-time end point control, thus addressing both the course correction and fault management aspects of advanced process control.

In conclusion, the demonstration of real-time process and wafer state metrology and its application to real-time end

point control opens a door to *real-time* advanced process control at a level of order 1% accuracy in deposition rate/thickness. The specific choice of mass spectrometry is beneficial in its capability to support existing fault detection applications and to advance course correction capability to a real-time domain.

ACKNOWLEDGMENTS

[1] *National Technology Roadmap for Semiconductors,* section on Materials and Bulk Processes (Semiconductor Industry Association, San Jose, 1994); *Metrology Roadmap: A Supplement to the National Technology Roadmap for Semiconductors,* section on Sensors and Methodology for *In-situ* Process Control, SEMATECH Technology Transfer Document No. 94102578A-TR.

[2] *1997 National Technology Roadmap for Semiconductors* (Semiconductor Industry Association, San Jose, 1998), Metrology Section, p. 183.

[3] M. Melliar-Smith and A. C. Diebold, AIP Conf. Proc. **449**, 3 (1998).

[4] S. W. Butler, AIP Conf. Proc. **449**, 47 (1998).

[5] S. W. Butler, J. Vac. Sci. Technol. B **13**, 1917 (1995).

[6] A. Toprac and W. J. Campbell, Semiconductor International, 2001 (unpublished).

[7] J. Baliga, Semiconductor International, 1999 (unpublished).

[8] L. L. Tedder, G. W. Rubloff, I. Shareef, M. Anderle, D.-H. Kim, and G. N. Parsons, J. Vac. Sci. Technol. B **13**, 1924 (1995).

[9] S. W. Butler, J. Hosch, A. C. Diebold, and B. Van Eck, Future Fab Int. **1**, 315 (1997).

[10] J. A. O'Neill, M. L. Passow, and T. J. Cotler, J. Vac. Sci. Technol. A **12**, 839 (1994).

[11] K.-I. Hanoaka, H. Ohnishi, and K. Tachibana, Jpn. J. Appl. Phys., Part 1 **32**, 4774 (1993).

[12] B. J. Rappoli and W. J. DeSisto, Appl. Phys. Lett. **68**, 2726 (1996).

[13] L. Henn-Lecordier, J. N. Kidder, Jr., G. W. Rubloff, C. A. Gogol, and A. Wajid, J. Vac. Sci. Technol. A **19**, 621 (2001).

[14] S. Yamamoto, K. Nagata, S. Sugai, A. Sengoku, Y. Matsukawa, T. Hattori, and S. Oda, Jpn. J. Appl. Phys., Part 1 **38**, 4727 (1999).

[15] X. Li, M. Schaepkens, G. S. Oehrlein, R. E. Ellefson, L. C. Frees, N. Mueller, and N. Korner, J. Vac. Sci. Technol. A **17**, 2438 (1999).

[16] G. Lu, L. L. Tedder, and G. W. Rubloff, J. Vac. Sci. Technol. B **17**, 1417 (1999).

[17] T. Gougousi, Y. Xu, J. N. Kidder, Jr., G. W. Rubloff, and C. Tilford, J. Vac. Sci. Technol. B **18**, 1352 (2000).

[18] M. L. Yu and B. N. Eldridge, J. Vac. Sci. Technol. A **7**, 625 (1989).

[19] J. Ammerlaan, Ph.D. thesis, Delft University of Technology, 1994.

[20] Y. Xu, Ph.D thesis, University of Maryland, 2000, PhD 2001-2 ISR Technical report, http://www.isr.umd.edu/TechReports/

[21] R. Sreenivasan, T. Gougousi, Y. Xu, J. N. Kidder, Jr., E. Zafiriou, and G. W. Rubloff, J. Vac. Sci. Technol. B **19**, 1931 (2001).